

UC Irvine

UC Irvine Previously Published Works

Title

Persistence analysis of velocity and temperature fluctuations in convective surface layer turbulence

Permalink

<https://escholarship.org/uc/item/262669qs>

Journal

Physics of Fluids, 32(7)

ISSN

1070-6631

Authors

Chowdhuri, Subharthi
Kalmár-Nagy, Tamás
Banerjee, Tirtha

Publication Date

2020-07-01

DOI

10.1063/5.0013911

Peer reviewed


Persistence analysis of velocity and temperature fluctuations in convective surface layer turbulence

Cite as: Phys. Fluids **32**, 076601 (2020); <https://doi.org/10.1063/5.0013911>

Submitted: 15 May 2020 . Accepted: 15 June 2020 . Published Online: 01 July 2020

Subharthi Chowdhuri , Tamás Kalmár-Nagy , and Tirtha Banerjee 

COLLECTIONS

 This paper was selected as Featured



View Online



Export Citation




CrossMark



NEW!

Sign up for topic alerts
New articles delivered to your inbox



Persistence analysis of velocity and temperature fluctuations in convective surface layer turbulence

Cite as: Phys. Fluids 32, 076601 (2020); doi: 10.1063/5.0013911

Submitted: 15 May 2020 • Accepted: 15 June 2020 •

Published Online: 1 July 2020



Subharthi Chowdhuri,^{1,a)}  Tamás Kalmár-Nagy,^{2,b)}  and Tirtha Banerjee^{3,c)} 

AFFILIATIONS

¹Indian Institute of Tropical Meteorology, Ministry of Earth Sciences, Dr. Homi Bhabha Road, Pashan, Pune 411008, India

²Department of Fluid Mechanics, Faculty of Mechanical Engineering, Budapest University of Technology and Economics, 4-6 Bertalan Lajos u, Budapest 1111, Hungary

³Department of Civil and Environmental Engineering, University of California, Irvine, California 92697, USA

^{a)} Author to whom correspondence should be addressed: subharthi.cat@tropmet.res.in

^{b)} Electronic mail: physfluids@kalmarnagy.com

^{c)} Electronic mail: tirthab@uci.edu

ABSTRACT

Persistence is defined as the probability that the local value of a fluctuating field remains at a particular state for a certain amount of time, before being switched to another state. The concept of persistence has been found to have many diverse practical applications, ranging from non-equilibrium statistical mechanics to financial dynamics to distribution of time scales in turbulent flows and many more. In this study, we carry out a detailed analysis of the statistical characteristics of the persistence probability density functions (PDFs) of velocity and temperature fluctuations in the surface layer of a convective boundary layer using a field-experimental dataset. Our results demonstrate that for the time scales smaller than the integral scales, the persistence PDFs of turbulent velocity and temperature fluctuations display a clear power-law behavior, associated with a self-similar eddy cascading mechanism. Moreover, we also show that the effects of non-Gaussian temperature fluctuations act only at those scales that are larger than the integral scales, where the persistence PDFs deviate from the power-law and drop exponentially. Furthermore, the mean time scales of the negative temperature fluctuation events persisting longer than the integral scales are found to be approximately equal to twice the integral scale in highly convective conditions. However, with stability, this mean time scale gradually decreases to almost being equal to the integral scale in the near-neutral conditions. Contrarily, for the long positive temperature fluctuation events, the mean time scales remain roughly equal to the integral scales, irrespective of stability.

Published under license by AIP Publishing. <https://doi.org/10.1063/5.0013911>

I. INTRODUCTION

Let $f(t)$ denote a stochastic signal fluctuating in time governed by a particular dynamics. The persistence is then the probability $P(t)$ that the quantity $f(t) - \overline{f(t)}$ does not change sign up to the time t ,^{1,2} where the overbar denotes the time average. Despite its simple description, only for some specific systems, such as those exhibiting fractional Brownian motions, the persistence probability density functions (PDFs) could be analytically shown to decay as a power-law, $P(t) \propto t^{-(1-H)}$. Here, H is the Hurst exponent ($0 < H < 1$) whose value of 0.5 indicates simple Brownian motion.^{1,3-5} The power-law

form of $P(t)$ dictates that as the H values get larger, the persistence PDFs decrease more slowly, which seems to be consistent with the general notion that a stochastic signal displays anti-persistent or persistent behavior depending on whether $0 < H < 1/2$ or $1/2 < H < 1$.⁶ However, for other complex systems, no theoretical solutions exist for the persistence PDFs, and these need to be computed empirically from the experimental data at hand.⁷ Notwithstanding the theoretical challenges, the concept of persistence has many practical applications, such as in the field of biology where one can ask how long does it take for an epidemic to spread,⁸ in financial markets to assess when does a preferred stock will cross a threshold price,⁹ or

in the field of geophysics to predict when will the next earthquake have a dangerously high magnitude.¹⁰ Note that, depending on the context, the persistence could also be referred to as distributions of the first-passage time, survival probability distributions, return-time distributions, or the distributions of the inter-arrival times between the successive zero-crossings.¹¹

In turbulent flows, the interest in the concept of persistence or zero-crossings grew with the analytical result from Rice¹² through which it was possible to show that the frequency of the zero-crossings in a turbulent signal was related to the Taylor microscale.¹³ This connection was intriguing because it implied that the dissipation rate of the turbulent kinetic energy could be directly computed from the zero-crossing frequencies. Since then, several studies are carried out in wall-bounded turbulent flows to verify this result, and the agreements obtained with the theoretical prediction are more or less satisfactory.^{13–16} However, there has been a fair amount of disagreement among different experiments regarding the statistical characteristics of the PDFs of the inter-arrival times between the successive zero-crossings (hereafter, the persistence PDFs). Narayanan, Rajagopalan, and Narasimha¹⁵ found that in a turbulent boundary layer, the persistence PDFs of the velocity fluctuations were log-normal to a good approximation. Later, Sreenivasan, Prabhu, and Narasimha¹³ and Kailasnath and Sreenivasan¹⁷ found that the persistence PDFs of the velocity fluctuations and momentum flux signals were double-exponential in nature. Their interpretation of this behavior was that the long intervals are a consequence of the large-scale structures passing the sensor and the short intervals are a consequence of the impinging small-scale motions superposed on the large-scale structures. Subsequently, Bershadskii *et al.*¹⁸ showed that the persistence PDFs of temperature fluctuations from a turbulent convection experiment followed a power-law distribution, which indicates scale-free behavior. In a follow up study, Sreenivasan and Bershadskii¹⁹ commented that when the temperature behaved like an active scalar in convective turbulence, the persistence PDFs followed a power-law distribution. On the other hand, when the temperature behaved like a passive scalar in shear-driven turbulence, the persistence PDFs followed a log-normal distribution. Recently, Kalmár-Nagy and Varga²⁰ noted that the persistence PDFs of velocity fluctuations followed a log-normal distribution in a turbulent flow around a street canyon.

In atmospheric turbulence, the investigation of the statistical properties of the persistence PDFs of turbulent fluctuations is quite rare. Nevertheless, there are a few limited studies available from the atmospheric surface layer, which report the persistence PDFs of velocity and scalar fluctuations.^{21–24} The atmospheric surface layer is a generalization of the inertial layer of unstratified wall-bounded flows by including the effect of buoyancy, where the effects of surface roughness are no longer important and the modulations by the outer eddies are not too strong.^{25,26} Yee *et al.*^{21,22} reported that the persistence PDFs of scalar concentrations displayed a double power-law in a near-neutral surface layer. Later, Katul *et al.*²⁷ also observed the same, when they investigated the persistence PDFs of the burst events in the sensible heat flux in a convective surface layer. Pinto, Lopes, and Tenreiro Machado²⁸ showed that the double power-law feature in a distribution function is related to the presence of two sets of fractals with two different fractal dimensions associated with two different scale-free processes. However, Narasimha *et al.*²⁹ found that the persistence

PDFs of the momentum flux events in a near-neutral surface layer followed an exponential distribution, suggestive of a Poisson type process. Recently, Cava and Katul²³ demonstrated that the persistence PDFs of the velocity and scalar fluctuations in a canopy surface layer turbulence could be power-laws with log-normal cutoffs or log-normal distributions depending on the measurement height in the canopy. In due course, Cava *et al.*²⁴ showed that the persistence PDFs of the velocity and scalar fluctuations in the canopy and atmospheric surface layer turbulence could be modeled as a power-law distribution with an exponential cutoff in convective conditions. Chamecki³⁰ lent support for this model by investigating the persistence PDFs of velocity fluctuations above and within a cornfield canopy.

Therefore, from this brief review, it is apparent that there is a very little consensus about the statistical characteristics of the persistence PDFs for both laboratory and atmospheric turbulent flows. Nevertheless, in a convective atmospheric surface layer, a detailed understanding of the persistence properties of velocity and temperature fluctuations is important since it holds the key to explain the quadrant cycles of the heat and momentum fluxes. This is because the switching patterns of the heat and momentum fluxes from one quadrant to the other are dependent on the zero-crossings of the component signals, as described by their persistence PDFs. Thus, we define our objectives for this study as follows:

1. To carry out a detailed analysis to establish the statistical scaling properties of the persistence PDFs of velocity and temperature fluctuations in a convective surface layer.
2. To empirically connect the statistical scaling properties of the persistence PDFs with the turbulent structures in a convective surface layer.

This study is organized as follows: In Sec. II, we provide the descriptions of the field-experimental dataset and methodology used in this study; in Sec. III, we present and discuss the results; and finally, in Sec. IV, we conclude by presenting our findings and providing the future research direction.

II. DATASET AND METHODOLOGY

In this study, the dataset being used is from the Surface Layer Turbulence and Environmental Science Test (SLTEST) experiment. The SLTEST experiment ran continuously for nine days from 26 May 2005 to 03 June 2005, over a flat and homogeneous terrain at the Great Salt Lake desert in UT, USA (40.14° N, 113.5° W), with the aerodynamic roughness length (z_0) being $z_0 \approx 5$ mm.³¹ During this experiment, nine north-facing time synchronized CSAT3 sonic anemometers were mounted on a 30-m mast, spaced logarithmically over an 18-fold range of heights, from 1.42 m to 25.7 m, with the sampling frequency being set at 20 Hz.

During the daytime convective periods, the standard practice is to compute the turbulent statistics in the atmospheric surface layer over a 30-min period.^{32–34} Therefore, the data from all nine sonic anemometers were restricted to rain-free daytime convective periods and subsequently being divided into 30-min sub-periods, containing the 20-Hz measurements of the three wind components and the sonic temperature.³⁵ To select the 30-min periods for the persistence analysis, we followed the detailed data selection methods as

TABLE I. The six different stability classes formed from the ratio $-\zeta = z/L$ in an unstable atmospheric surface layer flow, where z is the height above the surface and L is the Obukhov length. The ratios span from highly convective ($-\zeta > 2$) to near-neutral ($0 < -\zeta < 0.2$) conditions. The number of 30-min runs and the associated heights with each of the stability classes are given. The total numbers of zero-crossings (No. ZC) in u' , v' , w' , and T' signals associated with each stability class are also provided.

Stability class	Number of 30-min runs	Heights	u' (No. ZC)	v' (No. ZC)	w' (No. ZC)	T' (No. ZC)
$-\zeta > 2$	55	$z = 6.1$ m, 8.7 m, 12.5 m, 17.9 m, 25.7 m	116 459	86 576	142 751	127 633
$1 < -\zeta < 2$	53	$z = 3$ m, 4.3 m, 6.1 m, 8.7 m, 12.5 m, 17.9 m, 25.7 m	119 511	92 236	189 131	138 785
$0.6 < -\zeta < 1$	41	$z = 2.1$ m, 3 m, 4.3 m, 6.1 m, 8.7 m, 12.5 m, 17.9 m	97 575	73 884	184 652	115 173
$0.4 < -\zeta < 0.6$	34	$z = 1.4$ m, 2.1 m, 3 m, 4.3 m, 6.1 m, 8.7 m	90 551	70 957	193 302	107 356
$0.2 < -\zeta < 0.4$	44	$z = 1.4$ m, 2.1 m, 3 m, 4.3 m, 6.1 m	128 538	98 123	293 816	154 774
$0 < -\zeta < 0.2$	34	$z = 1.4$ m, 2.1 m, 3 m	114 383	95 228	285 961	143 470

outlined in Ref. 36. Note that we rotated the coordinate systems of all nine sonic anemometers in the streamwise direction by applying the double-rotation method of Kaimal and Finnigan³³ for each 30-min period.

A total of 261 combinations of the stability ratios ($-\zeta = z/L$, where L is the Obukhov length) were possible for the selected 30-min periods from the convective conditions ($-L > 0$). The stability ratio $-z/L$ is the ratio between the turbulent kinetic energy generated due to buoyancy and due to shear, with the Obukhov length (L) being defined as

$$L = -\frac{u_*^3 T_0}{k_v g H_0}, \tag{1}$$

where T_0 is the surface air temperature, g is the acceleration due to gravity (9.8 m s^{-2}), H_0 is the surface kinematic heat flux, k_v is the von Kármán constant (0.4), and u_* is the friction velocity. It is to be noted that these are the same set of runs used by Chowdhuri, Kumar, and Banerjee³⁶ for their study of turbulence anisotropy. The entire range of $-\zeta$ ($12 \leq -\zeta \leq 0.07$) was divided into six stability classes

and considered for the persistence analysis (see Table I). For each 30-min run, the turbulent fluctuations of the three velocity components in the streamwise (u'), cross-stream (v'), and vertical (w') directions along with the fluctuations in the sonic temperature (T') were computed by removing the linear trend from the 30-min period associated with the respective variables.³⁷

A graphical illustration of the persistence phenomenon is provided in Fig. 1, where a 120-s long section of u' signal is shown for a particular 30-min run, corresponding to a $-\zeta = 10.6$. Figure 1 shows that the u' signal displays persistent positive or negative (i.e., above or below the mean) values for a particular amount of time, denoted as t_p . Note that the persistence time t_p can also be interpreted as the inter-arrival time between the subsequent zero-crossings where the u' signal changes its sign. The zero-crossings are identified by using the telegraphic approximation (TA) of the u' signal as

$$(u')_{TA} = \frac{1}{2} \left(\frac{u'(t)}{|u'(t)|} + 1 \right) \tag{2}$$

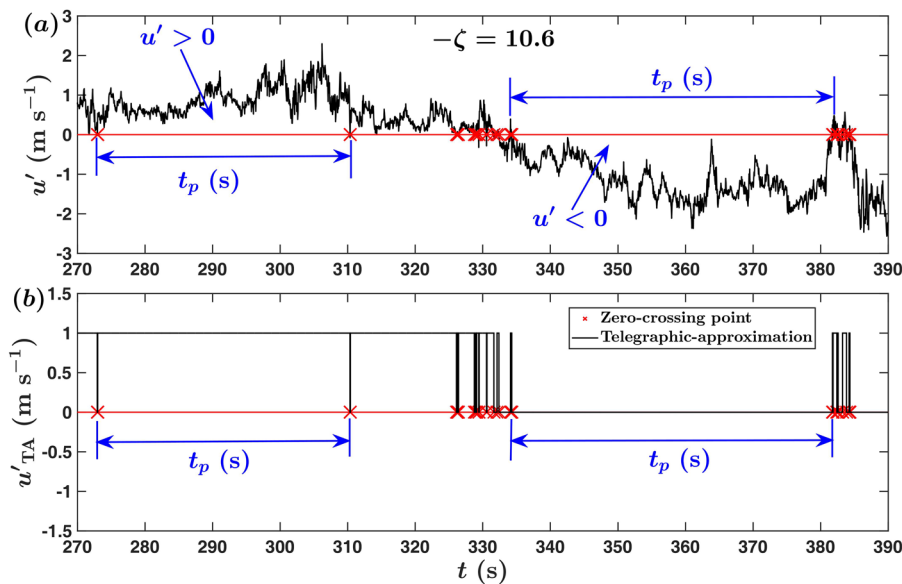


FIG. 1. A 120-s long section of a time series of u' from a highly convective surface layer corresponding to $-\zeta = 10.6$ is shown for (a) actual values and (b) its telegraphic approximation (TA), where $u' > 0$ is denoted as 1 and $u' < 0$ is denoted as 0. The red horizontal line denotes the position of zero, and the red crosses show the points where the u' signal changes its sign from positive to negative or vice versa (zero-crossings). To provide an example, two particular regions of the u' signal are highlighted where the positive and negative values persist for a time t_p (around 30 s–50 s).

and locating the points where the TA series changes its value from 0 to 1 or vice versa [see Fig. 1(b)]. The associated probability that the u' signal stays positive or negative for t_p amount of time can be evaluated by constructing the persistence PDFs using standard statistical procedures (see Appendix A). Moreover, the same concept can also be extended to other turbulent fluctuations such as v' , w' , and T' .

For any stability class as outlined in Table I, the number of persistent events (corresponding to each t_p values) in u' , v' , w' , and T' signals can be represented by the number of zero-crossings. In Table I, we provide the number of zero-crossings or persistent events by considering all the 30-min runs from a particular stability class. Typically, we encounter in the order of 10^5 , the number of zero-crossings for each signal from every stability class (see Table I). Therefore, the persistence PDFs of velocity and temperature fluctuations for each of these six stability classes are constructed over these large number of ensemble events to ensure their statistical robustness. In Sec. III, we discuss the properties of these persistence PDFs, corresponding to these six stability classes.

III. RESULTS AND DISCUSSION

Before describing the features of the persistence PDFs, it is worthwhile to discuss about the presentation of the results. Earlier studies by Narayanan, Rajagopalan, and Narasimha,¹⁵ Sreenivasan, Prabhu, and Narasimha,¹³ and Kailasnath and Sreenivasan¹⁷ on turbulent boundary layer flows have presented the results on persistence time scales after converting those to spatial length scales by employing Taylor's frozen turbulence hypothesis. It is important to note that although they presented results on the inter-arrival times between the two successive zero-crossings of turbulent signals, their convention is equivalent to persistence time t_p (see Fig. 1). They interpreted this spatial length scale as a representative of the eddy length scale of the flow, given the connection between the mean value of the zero-crossings with the Taylor microscale.^{13,14,17}

In the convective surface layer turbulence, it is a common practice to normalize the spatial length scales in the streamwise direction by the height above the surface.^{38–43} This is related to the assumption that the turbulent structures in a convective surface layer are self-similar with height.^{40,44–48} Thus, before computing the persistence PDFs, it seems apropos to convert the persistence time t_p to a streamwise length ($t_p \bar{u}$, where \bar{u} is the mean horizontal wind speed) by applying Taylor's frozen turbulence hypothesis and subsequently normalizing the same with z . Note that for all our selected runs, σ_u/\bar{u} (where σ_u is the standard deviation of the streamwise velocity) was less than 0.2, and so Taylor's frozen turbulence hypothesis could be assumed to be valid.⁴⁹ The normalized variable $(t_p \bar{u})/z$ has a large range, given that the minimum of t_p is restricted by the sampling interval of 0.05 s (20-Hz sampling frequency) and the maximum of t_p could go as large as in the order of 10^2 s (see Fig. 1). A well-suited strategy to evaluate the PDFs of such variables is to take the logarithmic transformation and then binning the transformed variables in the logarithmic space.^{50–57} More details about the effect of binning strategy on the persistence PDFs is provided in Appendix A.

Therefore, we begin with discussing the properties of the persistence PDFs of velocity and temperature fluctuations in a convective

surface layer by presenting the empirical results scaled with z . Subsequently, to develop a physical understanding of these persistence PDFs, we present comprehensive evidence to underpin their scaling properties and relate them with the turbulent flow structures.

A. Persistence PDFs of velocity and temperature fluctuations

In Fig. 2, we show the persistence PDFs of velocity (u' and w') and temperature fluctuation (T') signals, plotted against $(t_p \bar{u})/z$ for the six different stability classes outlined in Table I. These persistence PDFs ($P[(t_p \bar{u})/z]$) are computed after logarithmically binning the ensemble of values of $(t_p \bar{u})/z$ from a particular stability class and then using Eq. (A2) to take into account the effect of the variable bin-width owing to the logarithmic transformation (see Appendix A). The log-log representation is used in Fig. 2 such that the power-law functions on such plots would be represented by straight line segments.

Similar to Bershadskii *et al.*¹⁸ and Chamecki,³⁰ the persistence PDFs are computed separately for the positive and negative fluctuations (shown as blue and red markers in Fig. 2) for u' , w' , and T' signals and compared with the persistence PDFs for the total fluctuations (combining both positive and negative) shown as gray markers. Note that we focus on u' , w' , and T' signals since unraveling the characteristics of their persistence PDFs has an implication toward understanding the genesis of ejection and sweep cycles in streamwise momentum ($u'w'$) and heat flux ($w'T'$) signals. Nevertheless, the persistence PDFs of v' signals are shown in Fig. S1 of the supplementary material, and they display a similar characteristic shape as u' signals for all six stability classes.

From Fig. 2(a), one can note that under highly convective stratification regimes, an extensive straight line segment is observed in the persistence PDF of the u' signal with a cutoff at $(t_p \bar{u})/z \approx 10$. Moreover, the persistence PDFs of T' and w' signals also display a straight line segment for the small values of $(t_p \bar{u})/z$, although their extent remains shorter than the u' signal, with cutoffs at $(t_p \bar{u})/z \approx 4$ and $(t_p \bar{u})/z \approx 1$, respectively [Fig. 2(a)]. In the log-log representation, a straight line segment is reminiscent of a power-law function, thus indicating the persistence PDFs of u' , w' , and T' signals behave in a power-law fashion up to a certain threshold of $(t_p \bar{u})/z$. Note that the exponents of these power-law functions in Fig. 2(a) are different for u' , T' , and w' signals being equal to 1.6, 1.4, and 1.25, respectively. These exponents have been estimated from a linear regression on the log-log plots in Fig. 7, which we will revisit in Sec. III C while discussing the physical significance of this power-law behavior. Since power-laws are scale invariant, a different scaling of the persistence time t_p as employed in Fig. 7 would not affect their exponents.

To judge the effect of stability on the exponents of these power-law functions, we compared the exponents obtained from the highly convective stability [Fig. 2(a)] with the other five stability classes [Figs. 2(b)–2(f)]. We note that for the w' signal, with the change in stability, the extent of this power-law region gradually shrinks, becoming almost non-existent in the near-neutral stability [Figs. 2(a)–2(f)]. On the contrary, no discernible change is being observed in the power-law behavior of u' signals with stability. However, for T' signals, there is a modest change in the extent of the power-law region with stability, although not as clearly visible as in

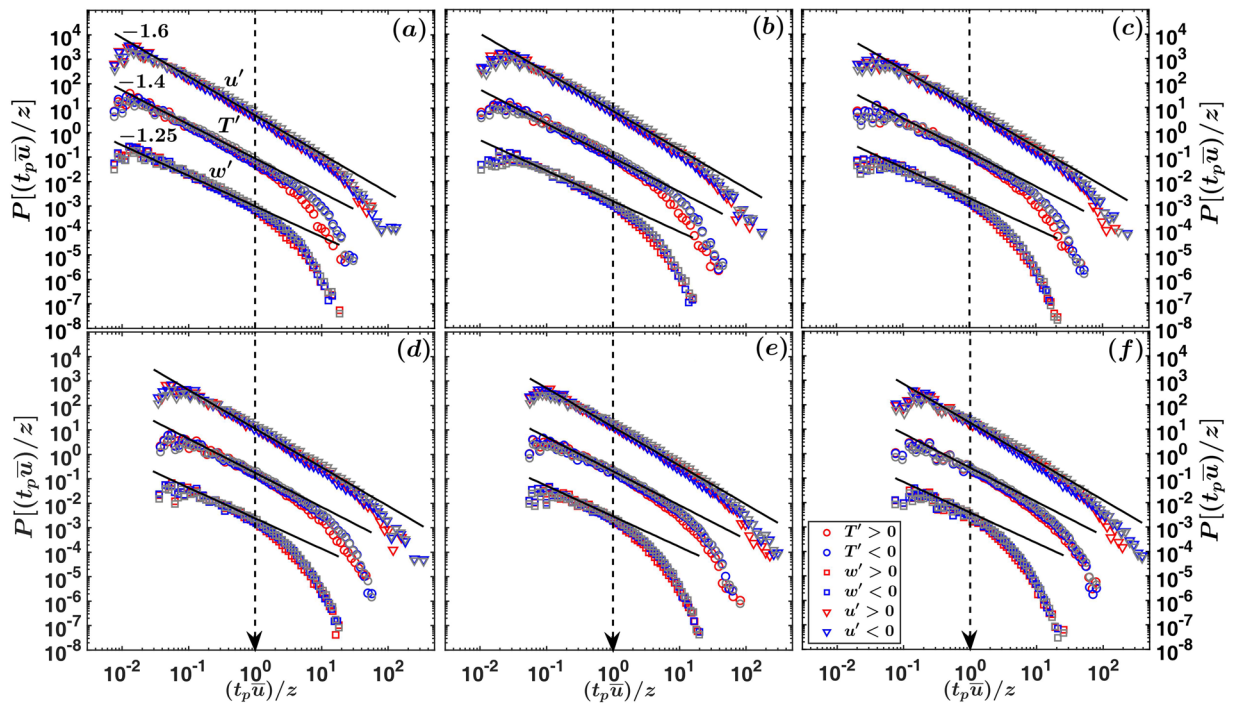


FIG. 2. The persistence PDFs of the normalized streamwise sizes $(t_p \bar{u})/z$ corresponding to the positive (red) and negative (blue) fluctuations in the streamwise velocity (u' , inverted triangles), temperature (T' , circles), and vertical velocity (w' , squares) are shown separately for the six different stability classes. The panels corresponding to these six stability classes are arranged from the top-left to the bottom-right as (a) $-\zeta > 2$, (b) $1 < -\zeta < 2$, (c) $0.6 < -\zeta < 1$, (d) $0.4 < -\zeta < 0.6$, (e) $0.2 < -\zeta < 0.4$, and (f) $0 < -\zeta < 0.2$. The gray inverted triangle, circle, and square markers on all the panels show the persistence PDFs computed after considering the positive and negative fluctuations together. The PDFs of w' , T' , and u' are shifted vertically by two decades for visualization purposes. The black thick lines on all the panels show the power-laws with their respective slopes being mentioned in panel (a). The black dashed line denotes the value of $(t_p \bar{u})/z = 1$.

the w' signal. Along with that, the threshold streamwise sizes up to which the power-law behavior holds are also not similar for these three signals. For the u' signal, at streamwise sizes greater than about $10z$, deviation from the power law is noted, whereas for the w' signal, the threshold streamwise size is much closer to z . On the other hand, for the T' signal, the threshold streamwise size is approximately in between of the sizes corresponding to u' and w' signals.

Additionally, we note that for u' and w' signals, the persistence PDFs of positive and negative fluctuations almost coincide with each other for all the values of $(t_p \bar{u})/z$. Nevertheless, the same is not true for the T' signal. It could be noted that for the highly convective stability class $[-\zeta > 2$, Fig. 2(a)], the persistence PDFs show a slight disparity between the positive and negative T' signals at the larger values of $(t_p \bar{u})/z$. However, this difference gradually disappears with the change in stability from highly convective to near neutral [Figs. 2(a)–2(f)]. Therefore, one may ask for highly convective stability, what causes this discrepancy between the persistence PDFs associated with positive and negative temperature fluctuations?

1. Linkage between the persistence PDFs and asymmetric distribution

To investigate the aforementioned question, it is useful to consider a premultiplied form of the persistence PDFs such as

$(t_p \bar{u})/z \times P[(t_p \bar{u})/z]$. From phenomenological arguments, we will show that such a form of the persistence PDF is equivalent to a time-fraction distribution associated with $(t_p \bar{u})/z$ by directly connecting the premultiplied persistence PDF with the PDF of the corresponding signal itself. We emphasize that such a connection is not possible to establish from the persistence PDFs alone (shown in Fig. 2) without considering its premultiplied form.

Therefore, to prove such a linkage, let us consider we have an N -member ensemble of $(t_p \bar{u})/z$ values corresponding to a signal in a particular state. Note that, in the present context, there are only two possible states where the signal could be either above or below the mean (positive or negative fluctuations). Since the persistence time is computed based on the number of points lying between successive zero-crossings multiplied by the sampling interval (see Fig. 1), we can write

$$\sum_{i=1}^Q [(t_p \bar{u})/z]_i n_i \propto T_f, \quad (3)$$

where Q is the number of unique members in the N -member ensemble of $(t_p \bar{u})/z$, n_i is the frequency of occurrences of these unique members, and T_f is the total time-fraction spent by the signal in that particular state. The right-hand side of Eq. (3) stems from the fact that the left-hand side of the same equation can be rearranged as

$$\sum_{i=1}^Q [(t_p \bar{u})/z]_i n_i = N \sum_{i=1}^Q [(t_p \bar{u})/z]_i P[(t_p \bar{u})/z] = N \overline{(t_p \bar{u})/z}, \tag{4}$$

where $P[(t_p \bar{u})/z] = (n_i/N)$ is the probability of selecting a unique member from the N -member ensemble. Given that the sum of all the possible t_p values is equal to the total time spent by the signal in a particular state and N, \bar{u} , and z are constants for a particular period, the quantity $N \overline{(t_p \bar{u})/z}$ in Eq. (4) is equivalent to T_f with some proportionality constants. Thus, from Eqs. (3) and (4), we can rewrite Eq. (3) in the integral form as

$$\int_{\left(\frac{t_p \bar{u}}{z}\right)_{\min}}^{\left(\frac{t_p \bar{u}}{z}\right)_{\max}} \left(\frac{t_p \bar{u}}{z}\right) P\left[\left(\frac{t_p \bar{u}}{z}\right)\right] d\left(\frac{t_p \bar{u}}{z}\right) \propto T_f. \tag{5}$$

Since Eq. (5) holds true for both positive and negative fluctuations, we may also rewrite Eq. (5) as

$$\int_{\left(\frac{t_p \bar{u}}{z}\right)_{\min}}^{\left(\frac{t_p \bar{u}}{z}\right)_{\max}} \left(\left[\frac{t_p \bar{u}}{z} P\left(\frac{t_p \bar{u}}{z}\right) \right]_N - \left[\frac{t_p \bar{u}}{z} P\left(\frac{t_p \bar{u}}{z}\right) \right]_P \right) d\left(\frac{t_p \bar{u}}{z}\right) \propto \Delta T_f, \tag{6}$$

where the subscripts P and N refer to the positive and negative fluctuations and ΔT_f is the difference in the time fractions associated with those. For a particular signal, the difference in time fractions associated with positive and negative fluctuations can be estimated from the PDF of that signal as

$$\left[\int_{-\infty}^0 p(\hat{x}) d\hat{x} - \int_0^{\infty} p(\hat{x}) d\hat{x} \right] = \Delta T_f, \tag{7}$$

where $p(\hat{x})$ is the PDF of the signal x normalized as $\hat{x} = x'/\sigma_x$ such that \hat{x} is a standard variable with zero mean and unit standard deviation. Through the cumulant expansion of Nakagawa and Nezu,⁵⁸ $p(\hat{x})$ can be expressed as

$$p(\hat{x}) = G(\hat{x}) \left[1 + \frac{\bar{\hat{x}}^3}{6} (\hat{x}^3 - 3\hat{x}) + \frac{1}{24} (\bar{\hat{x}}^4 - 3)(\hat{x}^4 - 6\hat{x}^2 + 3) \right] \tag{8}$$

$$G(\hat{x}) = \frac{1}{\sqrt{2\pi}} \exp\left(-\frac{\hat{x}^2}{2}\right),$$

where $G(\hat{x})$ is the standard Gaussian distribution and $\bar{\hat{x}}^3$ and $\bar{\hat{x}}^4$ are the skewness and kurtosis of the signal x . Katul *et al.*⁵⁹ showed that if the kurtosis is ignored in Eq. (8), then the left-hand side of Eq. (7) can be analytically evaluated as

$$\int_{-\infty}^0 p(\hat{x}) d\hat{x} = \frac{6 + (\sqrt{2/\pi}) \bar{\hat{x}}^3}{12}, \tag{9}$$

$$\int_0^{\infty} p(\hat{x}) d\hat{x} = \frac{6 - (\sqrt{2/\pi}) \bar{\hat{x}}^3}{12}.$$

By replacing the result from Eq. (9) in Eq. (7), we can write Eq. (6) as

$$\int_{\left(\frac{t_p \bar{u}}{z}\right)_{\min}}^{\left(\frac{t_p \bar{u}}{z}\right)_{\max}} \left(\left[\frac{t_p \bar{u}}{z} P\left(\frac{t_p \bar{u}}{z}\right) \right]_N - \left[\frac{t_p \bar{u}}{z} P\left(\frac{t_p \bar{u}}{z}\right) \right]_P \right) d\left(\frac{t_p \bar{u}}{z}\right) \propto \frac{\bar{\hat{x}}^3}{3\sqrt{2\pi}}. \tag{10}$$

Hence, from Eqs. (6)–(10), we conclude that the difference between the positive and negative fluctuations in the premultiplied form of the persistence PDFs is directly related to the non-Gaussian characteristics of the signal, approximated by its skewness. In addition to this, we also note that by performing a change of variables, Dorval⁵⁶ showed that the premultiplied PDF of a stochastic variable x is equivalent to the PDF of $\log(x)$, known as the logarithmic PDF (see Appendix A for further details).

2. Premultiplied or logarithmic persistence PDFs of velocity and temperature fluctuations

Figure 3 shows the logarithmic PDFs of $(t_p \bar{u})/z$ for the same six different stability classes shown in Fig. 2. These PDFs are computed after taking the logarithm of $(t_p \bar{u})/z$ in base 10 and dividing the fraction of samples by the logarithmic bin-width $d \log_{10}[(t_p \bar{u})/z]$. Similar to Fig. 2, in Fig. 3, the logarithmic persistence PDFs are shown separately for the positive and negative fluctuations and compared with the total fluctuations (combining both positive and negative), corresponding to u' , w' , and T' signals. Note that owing to premultiplication, the power-law sections of the premultiplied PDFs are comparatively flattened, whereas exaggeration occurs at the larger values of $(t_p \bar{u})/z$ (for a clear demonstration, see Fig. 8 in Appendix A).

From Fig. 3(a), we note that in highly convective stability, the premultiplied PDFs of the positive and negative T' signals are clearly separated at larger values of $(t_p \bar{u})/z > 4$ [shown by the divergence between the red and blue circles in Fig. 3(a)]. However, they agree with each other at the smaller values of $(t_p \bar{u})/z$. Using Eq. (10), we can conclude that this difference between positive and negative T' signals at the large values of $(t_p \bar{u})/z$ is related to the non-Gaussian characteristics of the temperature fluctuations, expressed by its skewness. Chowdhuri, Kumar, and Banerjee³⁶ noted that the skewness and kurtosis of the temperature fluctuations are strongly non-Gaussian (≈ 1.5 and 5, respectively) in the local free-convection limit ($-\zeta > 1$). This observation is in agreement with the previous studies in the convective surface layer.^{60–63} Our results show that this non-Gaussianity in the T' signal is only realized at large sizes of persistent temperature patterns, approximately greater than four times the measurement height.

It is also interesting to note that the total time fractions at these large sizes are governed by the negative fluctuation patterns alone [Fig. 3(a)]. Katul *et al.*⁵⁹ showed that the difference in the PDFs between the positive and negative T' signals could be attributed to the asymmetry between the warm-updraft and cold-downdraft motions under the assumption that the contributions from the counter-gradient quadrants could be ignored. Therefore, this finding is consistent with that of Adrian, Ferreira, and Boberg,⁶⁴ where they showed from laboratory experiments that in highly unstable conditions, the temperature fluctuation patterns are governed by the more frequent cold-downdrafts bringing well-mixed air from aloft, interspersed with intermittent occurrences of the warm-updraft motions rising from the ground.

However, this clear disparity between the premultiplied PDFs of positive and negative T' signals gradually disappears as the near-neutral stability is approached [Figs. 3(a)–3(f)]. This is congruous with the close to Gaussian characteristics of the T' signal in the near-neutral stability.^{65,66} Apart from that, for u' and w' signals, no difference is observed between the premultiplied PDFs of positive

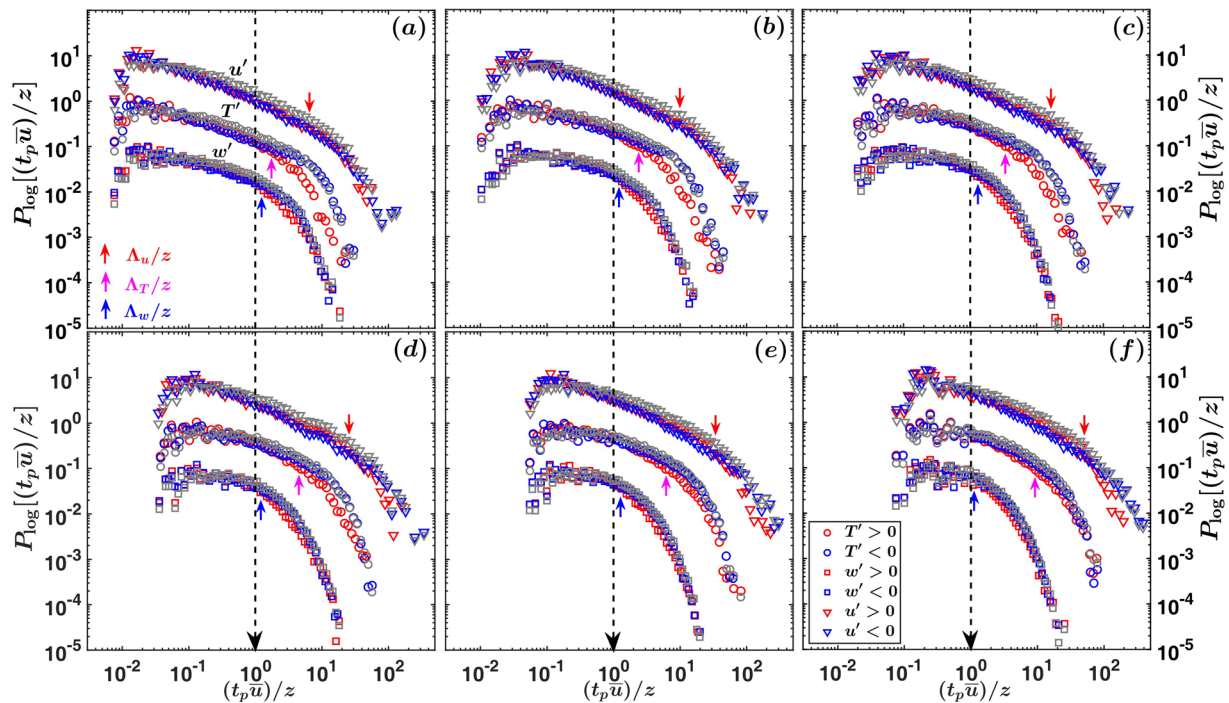


FIG. 3. Same as in Fig. 2, but for the logarithmic persistence PDFs of the normalized streamwise sizes $(t_p \bar{u})/z$. The panels corresponding to the six stability classes are arranged from the top-left to the bottom-right as (a) $-\zeta > 2$, (b) $1 < -\zeta < 2$, (c) $0.6 < -\zeta < 1$, (d) $0.4 < -\zeta < 0.6$, (e) $0.2 < -\zeta < 0.4$, and (f) $0 < -\zeta < 0.2$. The logarithmic PDFs of w' , T' , and u' are shifted vertically by a decade for visualization purposes. The colored arrows on all the panels show the position of the normalized integral length scales, corresponding to w' (blue arrows), T' (pink arrows), and u' (red arrows) signals.

and negative fluctuations, irrespective of the stability classes. The reason for this is that the PDFs of u' and w' signals remain very nearly Gaussian for all the stability conditions in an atmospheric surface layer.^{36,60}

In summary, for the convective surface layer turbulence, the persistence PDFs of the velocity and temperature fluctuations follow a power-law function up to a certain threshold size. This threshold size and the power-law exponents are not similar for u' , w' , and T' signals. For u' signals, the threshold size is an order of magnitude larger than z , whereas for w' signals, it is approximately equal to z . On the other hand, the threshold size for T' signals is somewhere in between of u' and w' signals. It is also remarkable to note that in a convective surface layer, the non-Gaussian effects in T' signals are only perceived at those sizes that are larger than this threshold size, where the power-law behavior ceases to exist. Therefore, it is imperative to ask in convective surface layer turbulence:

1. What statistical properties of velocity and temperature fluctuations give rise to the power-law behavior punctuated with a cutoff in their persistence PDFs?
2. How are those statistical properties connected with the structures of the turbulent flow?

In Secs. III B and III C, we will explore these questions by analyzing surrogate datasets and employing an alternate scaling of persistence time scales of velocity and temperature fluctuations.

B. Scrutiny of persistence PDFs through surrogate data

The persistence PDFs are related to the inter-arrival time between the successive zero-crossings of a time series. If these zero-crossings were randomly located being independent of each other, we would have expected the persistence PDFs to follow a Poisson distribution, which is exponential in nature.^{1,67} However, in a convective surface layer, the persistence PDFs of the turbulent velocity and temperature fluctuations show a power-law structure. This indicates the zero-crossings of these signals are not independent but correlated with each other. Moreover, for T' signals, the power-law behavior extends up to a certain streamwise size ($\approx 4z$) beyond which the non-Gaussian effects dominate the characteristics of the persistence PDFs.

Therefore, to gain more insight regarding the statistical characteristics of the persistence PDFs of u' , w' , and T' signals in convective turbulence, we generated the following two different types of surrogate datasets:

1. The temporal correlation of the original time series is preserved by keeping the auto-correlation function unchanged, but modifying the PDF of the time series to be Gaussian.
2. The temporal correlation of the original time series is destroyed by random shuffling, but keeping the PDF of the time series unchanged.

The normal procedure to generate the first type of the surrogate dataset is taking the Fourier transform of the time series and keeping the Fourier amplitudes the same but randomizing the associated Fourier phases, with inverse Fourier transform being applied to the modified Fourier coefficients.^{68,69} Since the Fourier amplitudes of the surrogate dataset are kept intact during the process of Fourier phase-randomization (PR), this procedure preserves the Fourier spectrum and hence the auto-correlation function of the time series. On the other hand, the second type of the surrogate dataset is generated by randomly permuting (shuffling) the original time series such that the temporal correlations are destroyed completely.

1. Phase-randomization and randomization experiments

For our purpose, we performed the phase-randomization and randomization experiments by varying the strength of the randomization to investigate their gradual effects on the behavior of the persistence PDFs. A similar procedure was suggested by Maiwald *et al.*⁷⁰ to investigate the effect of the non-linearity on a stochastic time series by increasing the strength of the phase-randomization in a step-wise manner. In this context, the randomization strength implies the percentage of the Fourier phases or the time series values that have been shuffled randomly to generate the surrogate datasets (see Appendix B for further details). Figure 4 shows the typical results from these two experiments for the highly convective stability class. Note that similar results have been found for the other five stability classes as well, which are not shown here. For illustration purposes, the logarithmic persistence PDFs of positive and negative T' signals are shown at various randomization strengths from 0% (original time series) to 100% (completely randomized) for phase-randomization [Fig. 4(a)] and randomization experiments [Fig. 4(b)], respectively (see Figs. S2 and S3 of the supplementary material for the effect on u' and w' signals). The logarithmic

representation is chosen, since, in this representation, the non-Gaussian characteristics of T' signals are better revealed while preserving the power-law structure of the persistence PDFs (Figs. 3 and 8).

From Fig. 4(a), we note that the power-law structure of the T' persistence PDFs are preserved for all the randomization strengths of the phase-randomization experiments, although the separation between the positive and negative T' persistence PDFs becomes indistinguishable at 20% randomization strength. This is related to the fact that in phase-randomization experiments, the surrogate time series of temperature fluctuations approach an almost Gaussian distribution at even 20% randomization strength [see Fig. S4(a) of the supplementary material]. On the contrary, from Fig. 4(b), we note that the power-law structure of the T' persistence PDFs gradually disappears as the strength of the randomization is increased to 100%. Nevertheless, in Fig. 4(b), the difference between the positive and negative T' persistence PDFs remains preserved, irrespective of the randomization strength. The reason for this is that the non-Gaussian PDFs of the temperature fluctuations remain unchanged in the randomization experiments [see Fig. S4(b) of the supplementary material]. Similar results are also obtained for the persistence PDFs of u' and w' signals (see Figs. S2 and S3 of the supplementary material).

To summarize the results from Fig. 4, we can conclude that the power-law behavior of the persistence PDFs is related to the temporal coherence in the time series. In a turbulent time series, the temporal coherence can be described by the integral time scale, defined as the time up to which the signal remains auto-correlated with itself.^{33,45,71}

2. Auto-correlation functions and integral scales

Figure 5 shows the auto-correlation functions [$R_{xx}(\tau)$, where x can be u' , w' , or T' signals and τ is the time lag] of u' , w' , and T' signals, plotted against the lags for the six different stability classes.

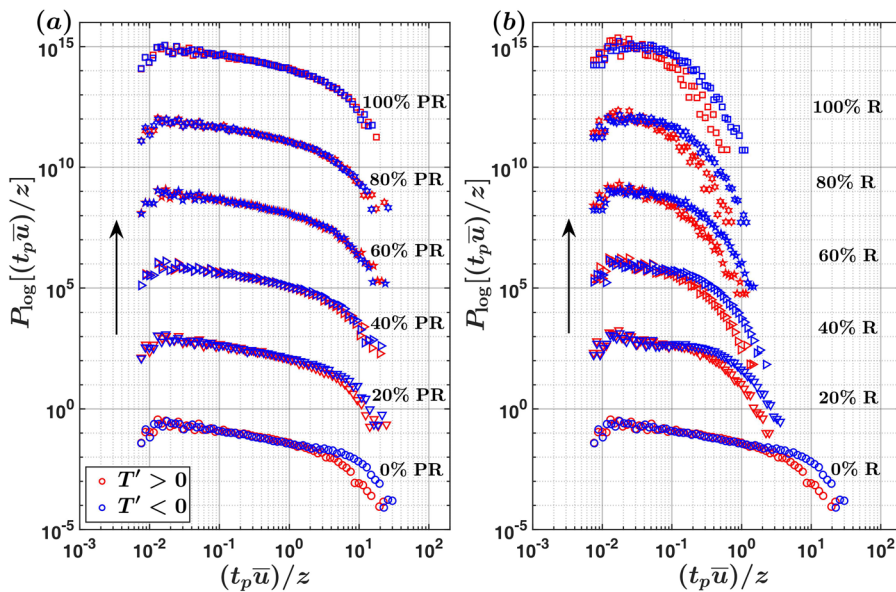


FIG. 4. The logarithmic persistence PDFs of the normalized streamwise sizes $(t_p \bar{u})/z$ corresponding to the positive (red) and negative (blue) fluctuations in the temperature (T') signal from the highly convective stability class ($-\zeta > 2$) are shown for the following two sets of experiments: (a) Fourier phase-randomization (PR) and (b) temporal randomization (R). The original logarithmic persistence PDFs are shown at the bottom of both the panels and the rest are shifted vertically by three decades where the original temperature signals are gradually randomized either in their Fourier phases or temporal values, starting from 20% to 100%.

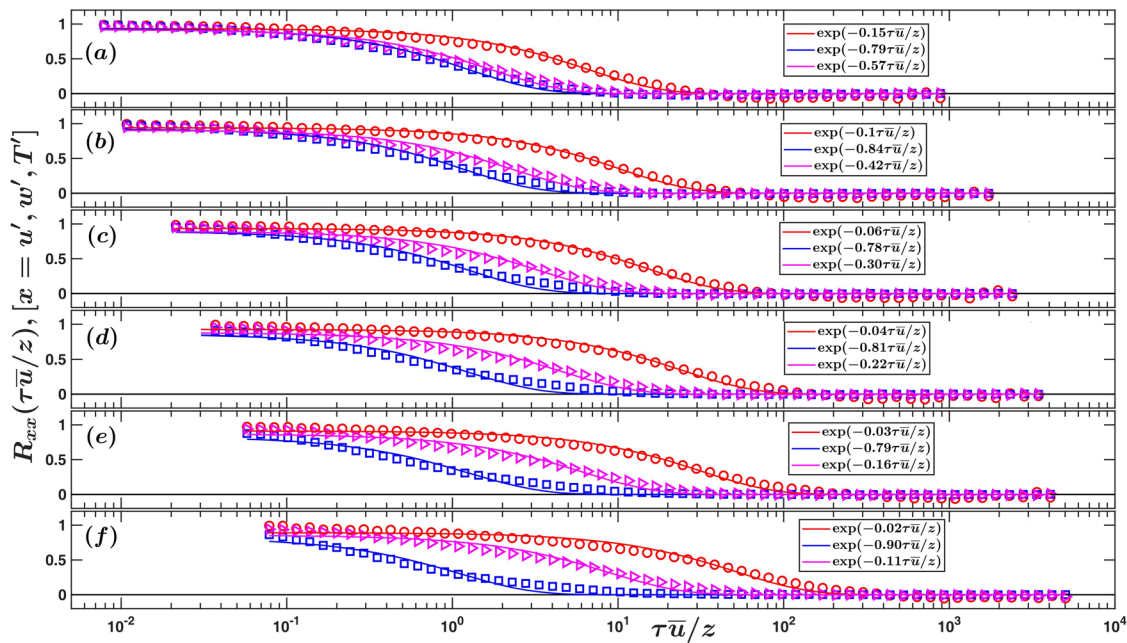


FIG. 5. The auto-correlation functions are plotted against the normalized time lags ($\tau\bar{u}/z$) for u' (red circles), w' (blue squares), and T' (pink inverted triangles) signals for the six different stability classes. The panels corresponding to these six stability classes are arranged from the top to the bottom as (a) $-\zeta > 2$, (b) $1 < -\zeta < 2$, (c) $0.6 < -\zeta < 1$, (d) $0.4 < -\zeta < 0.6$, (e) $0.2 < -\zeta < 0.4$, and (f) $0 < -\zeta < 0.2$. The exponential functions are fitted to the auto-correlation functions to determine the integral length scale associated with u' , w' , and T' signals. The legends shown in each panel describe the equations for the exponential fits.

Note that in Fig. 5, the time lags are converted to a streamwise length ($\tau\bar{u}$) by using Taylor's frozen turbulence hypothesis and normalized with z . Apart from that, the auto-correlation functions are ensemble averaged over the set of 30-min runs from a particular stability class (see Table I) to ensure that the results are statistically robust. These auto-correlations can be represented with an exponentially decaying function of the form

$$R_{xx}\left(\frac{\tau\bar{u}}{z}\right) = \exp\left(-K\frac{\tau\bar{u}}{z}\right) \implies \exp\left(-\frac{\ell_x}{\Lambda_x}\right), \quad (11)$$

where x can be u' , w' , or T' , $\ell_x = \tau\bar{u}$, and $\Lambda_x = z/K$, known as the integral length scale.³³

From Fig. 5(a), we note that the coefficients K for T' and w' signals are closer to each other ($K = 0.57$ and 0.79 , respectively), whereas the K value for the u' signal remains much lower ($K = 0.15$). Using Eq. (11), this implies that in the highly convective stability, the integral length scales of T' and w' signals ($\Lambda_x = z/K$) almost coincide with each other, while the integral length scale of the u' signal remains the largest. However, as the stability changes from highly convective to near neutral, the coefficients K of T' signals become closer to u' signals, implying that the Λ_T values approach Λ_u [Figs. 5(a)–5(f)]. On the other hand, the Λ_w values remain approximately equal to z , irrespective of the stability classes ($K = 0.79$ to 0.90).

These results are in accordance with the previous studies in surface layer turbulence, where it has been noted that in highly convective stability, the Λ_T values approach Λ_w , whereas in the near-neutral stability, they are much closer to Λ_u .^{39,72,73} Apart from

that, the approximate equality of Λ_w with z supports the argument that the eddies that contribute to the w' signal are attached to the ground.^{35,42,74,75} If these integral length scales obtained from Fig. 5 (Λ_u , Λ_w , and Λ_T) are replaced in the persistence length scales ($t_p\bar{u}$) in Fig. 3, we note that the deviation from the power-law occurs at those scales larger than the integral scales for u' , w' , and T' signals. The integral length scales are comparable to the peak wavelength of the turbulence energy spectrum.³³ This is demonstrated in Fig. S5 of the supplementary material for the highly convective stability class ($-\zeta > 2$), where the scaled peak wavenumbers (κz , where κ is the streamwise wavenumber) of the u' , w' , and T' spectra match with z/Λ_x (x can be u' , w' , or T' signals). Therefore, it indicates that the power-law behavior of the persistence PDFs is connected to the eddies from the inertial subrange of the turbulence spectra (sizes smaller than the integral scales). On the other hand, deviation from the power-law behavior in the persistence PDFs occurs at those scales comparable to the energy containing scale of eddies (sizes larger than the integral scales). To further explore this connection with the turbulent flow structures, it is appropriate to represent the persistence PDFs by scaling their persistence times with the integral scales. We present the results regarding those in Sec. III C.

C. Scaling the persistence time by the integral scales

We begin with discussing the logarithmic persistence PDFs, since in that representation, the disparity between the PDFs corresponding to the positive and negative fluctuations at larger

persistence scales is highlighted more clearly (see Fig. 3 in Sec. III A). The persistence time t_p of u' , w' , or T' signals are scaled with the integral time scale (Γ) before computing the logarithmic persistence PDFs. Note that from the application of Taylor's frozen turbulence hypothesis, this is equivalent to scaling the persistence length with integral scales Λ .

1. Logarithmic persistence PDFs

Figure 6 shows the logarithmic persistence PDFs with the persistence times normalized by Γ corresponding to u' , w' , or T' signals for all six stability classes (Table I). For all three signals in Fig. 6, a bend could be clearly observed in the logarithmic persistence PDFs at the time scales larger than the integral scales, indicating the clear deviation from the power-law. Apart from that, one can note from Fig. 6(a) (highly convective stability) that the difference between the positive and negative persistence PDFs for T' signals occurs exactly at those time scales that are larger than the integral time scales of temperature [see the gray region in Fig. 6(a)]. This discrepancy gradually disappears in near-neutral stability [see Figs. 6(a)–6(f)], implying that the non-Gaussian characteristics of the T' signal are definitely related to the energy containing scales of motions.

However, the persistence PDFs deviate from the power-law form at scales larger than the integral scales. Chamecki³⁰ showed, for canopy surface layer turbulence, the persistence PDFs of velocity fluctuations at large time scales behave exponentially, the hallmark of a random Poisson type process. Cava *et al.*²⁴ hypothesized this as a consequence of random deformation of the coherent

structures, giving rise to several sub-structures with independent arrival times. Nevertheless, Chamecki³⁰ also commented that this exponential nature of the persistence PDFs could be better studied by considering the cumulative distribution functions (CDFs), given their smoothed nature at large time scales.

The CDF [$F(t_p/\Gamma)$] is defined as

$$F(t_p/\Gamma) = \int_{(t_p/\Gamma)_{\max}}^{(t_p/\Gamma)} P(t_p/\Gamma) d(t_p/\Gamma), \quad (12)$$

which denotes the probability that the normalized persistence time has a value smaller than or equal to t_p/Γ . From Eq. (12), it follows that for an exponential distribution (Poisson process), both the PDFs and CDFs have the same form, albeit with different proportionality constants. Additionally, the CDFs also have an inherent advantage of being bin-independent with a smooth convergence toward 1.^{51,55}

At the right-hand side of Fig. 6 (see the side panels), the CDFs corresponding to the positive and negative T' signals are shown for the time scales larger than the integral scale Γ_T [$(t_p/\Gamma_T) > 1$] in a log-linear coordinate system, corresponding to all six stability classes (the CDFs of u' , w' , and T' signals for the whole range of t_p/Γ are provided in Fig. S6 of the supplementary material). The exponential decay of the CDFs,

$$F(t_p/\Gamma) \propto \exp[-\lambda(t_p/\Gamma)], \quad (13)$$

in such plots would appear as a straight line with the slope of λ .

For the highly convective stability [panel (a) at the right-hand side of Fig. 6], we note that the λ values obtained from the slopes

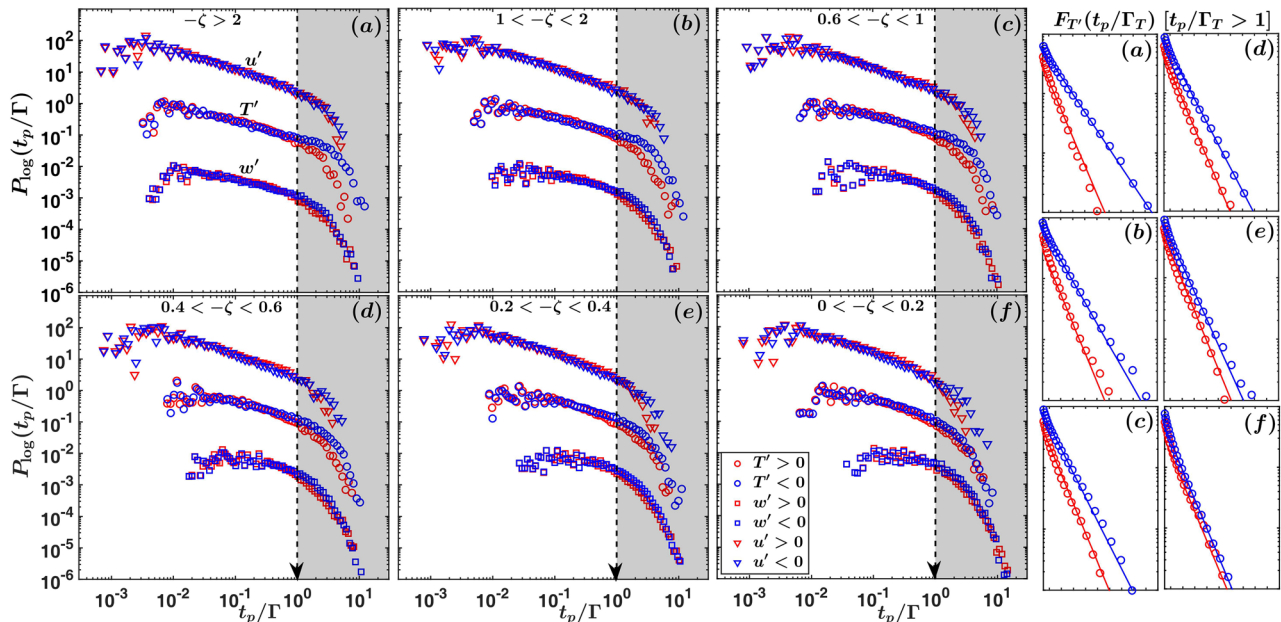


FIG. 6. The logarithmic persistence PDFs are shown for the persistence times normalized by the integral time scales (Γ) associated with w' (squares), T' (circles), and u' (inverted triangles) signals. The logarithmic PDFs are shifted vertically for visualization purposes. The panels on the right show the cumulative distribution functions of T' signals [$F_{T'}(t_p/\Gamma_T)$] plotted for $t_p/\Gamma_T > 1$ (marked as the gray regions on the left panels) on a log-linear plot. This representation is chosen to determine the slope of the exponential functions [represented as straight lines, see Eq. (13)] fitted separately for the positive and negative temperature fluctuations persisting for times larger than the integral time scales. The descriptions of the markers are shown in the legend, placed in a corner of the bottom panel (f) at the left-hand side.

of the straight line fits for negative and positive T' are 0.7 and 1.1, respectively. It implies that the mean time scales (Γ/λ) related to the long persistent events of negative T' are almost twice the integral scale of temperature, whereas for the positive T' , they are almost equal to the integral scale. Furthermore, with the change in stability from highly convective to near neutral, the λ values for the long events of positive T' remain fixed at 1.1, but for the negative T' , these values gradually increase from 0.7 to 1.1 at near-neutral stability [see the side panels (a)–(f) in Fig. 6]. This indicates that the mean time scales of the long persistent events of negative temperature fluctuations become closer to the integral scale of temperature as the near-neutral stability is approached, while the same remains unchanged for the positive fluctuation patterns.

Since these long events are associated with the energy containing scales (see Sec. III B), the disparity in the mean time scales (or length scales from Taylor’s frozen turbulence hypothesis) between the warm and cold events could be explained from the coherent structure perspective. The large-eddy simulation (LES) results of Khanna and Brasseur⁷⁶ and Salesky, Chamecki, and Bou-Zeid⁷⁷ indicate that in highly convective stability, the vertical velocity and temperature fluctuations display a cellular organization pattern. This explains the closeness of the integral scales of w' and T' in highly convective stability [Fig. 5(a)]. Apart from that, their LES simulations also show that the warm-updraft motions are concentrated at the cell edges, while the cold-downdraft motions occupy a larger area

at the cell center. This geometrical asymmetry between the warm-updraft and cold-downdraft motions might be the reason why the long warm events have mean length scales comparable to the integral scales, while the scales of the long cold events are almost twice of that. However, in near-neutral conditions, the warm and cold fluids are positioned on the long streaky patterns of streamwise fluctuations having similar streamwise lengths, comparable to the integral scales.^{76,77} Given the closeness of Λ_T and Λ_u in the near-neutral stability [Fig. 5(f)], this elucidates why in such conditions an equivalence is observed between the mean length scales of long warm and cold events.

2. Persistence PDFs

So far in Fig. 6, we have focused on the characteristics of the long persistent events larger than the integral scales (associated with energy containing eddies) by investigating the logarithmic representation of the persistence PDFs. However, it would also be advantageous to focus on the power-law structure of the persistence PDFs at scales smaller than the integral scales (associated with the eddies from the inertial subrange). Since the power-law behavior is best represented in the original PDFs, Fig. 7 shows the persistence PDFs of u' , w' , and T' signals with t_p scaled with Γ .

From Fig. 7, one can note the cut-off scale, where the deviation from the power-law behavior begins, is located almost exactly at the integral scale Γ for all three signals. Apart from that, compared to Fig. 2, the cut-off behavior of the power-law is quite sharp

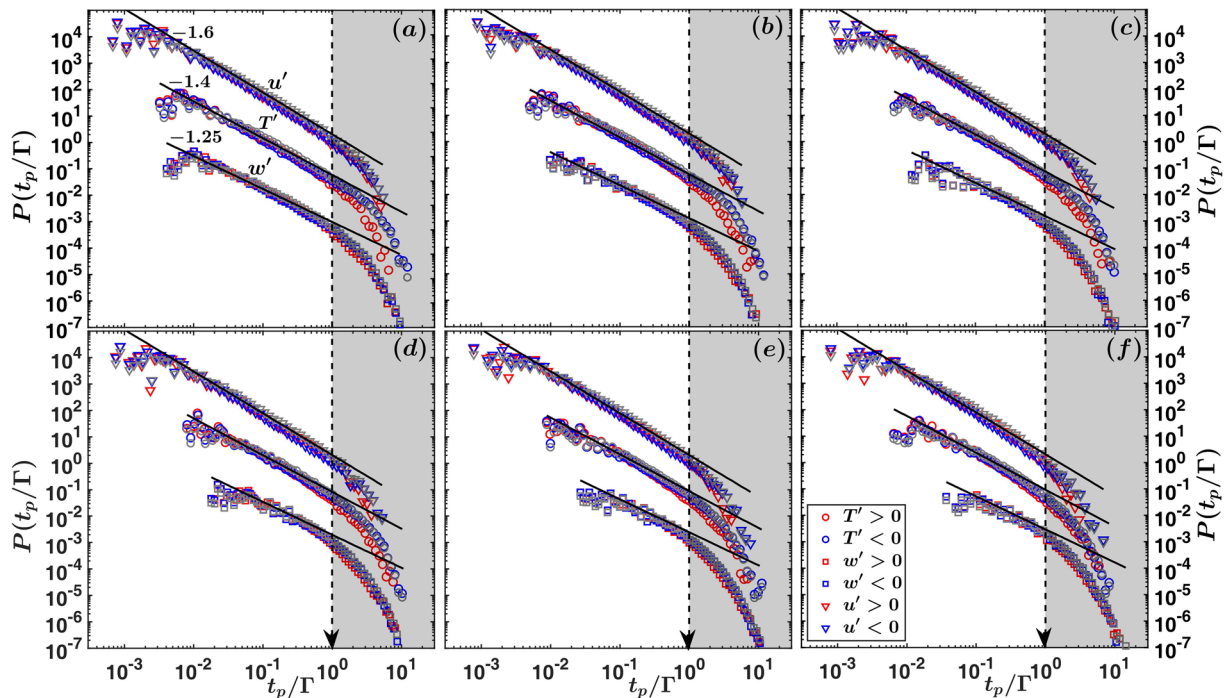


FIG. 7. The persistence PDFs are shown for the persistence times normalized by the integral time scales (Γ) associated with w' (squares), T' (circles), and u' (inverted triangles) signals. The panels corresponding to these six stability classes are arranged from the top-left to the bottom-right as (a) $-\zeta > 2$, (b) $1 < -\zeta < 2$, (c) $0.6 < -\zeta < 1$, (d) $0.4 < -\zeta < 0.6$, (e) $0.2 < -\zeta < 0.4$, and (f) $0 < -\zeta < 0.2$. The black thick lines on all the panels show the best fit power-laws with their respective slopes being mentioned in panel (a). The regions in all the panels corresponding to $t_p/\Gamma > 1$ are in gray. The descriptions of the markers are provided in the legend of panel (f).

in Fig. 7 due to the correct scaling of t_p with Γ . This feature is consistent with Fig. 6. Nevertheless, since the PDFs in Fig. 6 are in the premultiplied form, the exponents of the power-law for the scales smaller than the integral scales cannot be estimated from there (see Fig. 8 in Appendix A). Therefore, in Fig. 7(a) (highly convective stability), the exponents of the power-law functions are determined by performing a linear regression for the range $0.01 \leq t_p/\Gamma \leq 1$ on the log-log plots. The slopes (exponents) of the best fit lines are found to be 1.6, 1.4, and 1.25 for u' , w' , and T' signals, respectively, with R^2 values more than 0.98. Note that the exponent 1.4 for the T' signal is very close to 1.37 as reported by Bershanskii *et al.*¹⁸ from their turbulent convection experiments. To assess the effect of stability on the power-law behavior, the exponents obtained from the highly convective stability are compared with the other stability classes. The following features emerge:

1. For the u' signal, no change in the power-law behavior is observed with stability.
2. For the T' signal, no discernible change can be observed, although at near-neutral stability, a slight deviation from 1.4 exponent might be possible.

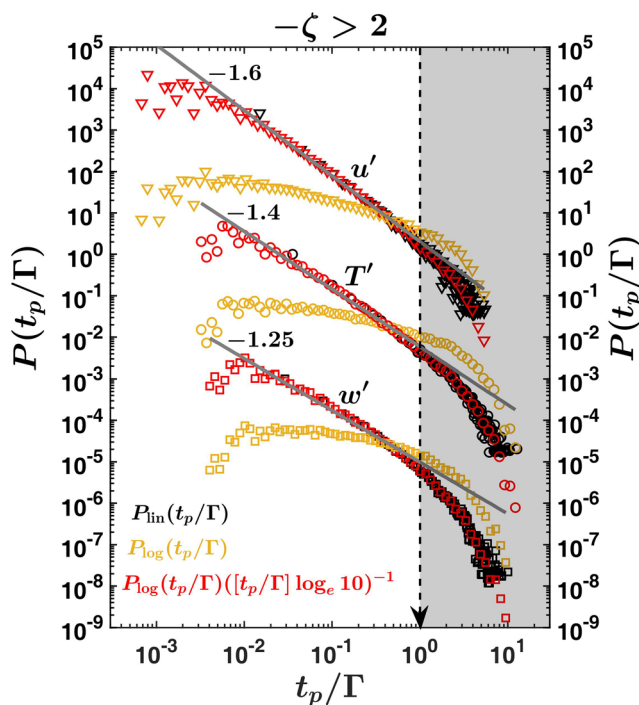


FIG. 8. An example is provided from the highly convective stability class ($-\zeta > 2$) to illustrate the effect of linear and logarithmic binning on the persistence PDFs of w' (squares), T' (circles), and u' (inverted triangles) signals, considering both the positive and negative fluctuations. The persistence times are normalized by the integral time scales (Γ) associated with w' , T' , and u' signals. The black markers indicate the persistence PDFs constructed from linear binning, whereas the orange markers denote the same but from logarithmic binning. To convert from logarithmic to linear space, the logarithmic persistence PDFs are premultiplied with the factor obtained from Eq. (A2) and are shown as the red markers. Note that all three PDFs for w' , T' , and u' signals are shifted vertically by three decades for visualization purposes. The gray thick lines show the same power-laws as in Figs. 2 and 7.

3. For the w' signal, the extent of the power-law behavior gradually decreases with stability.

Since the power-law structure in the persistence PDFs is associated with the t_p values smaller than the integral time scales, it is thus representative of the eddies from the inertial subrange of the turbulence spectrum. This observation lends considerable support to the hypothesis of Yee *et al.*²² and Cava *et al.*²⁴ where they connected this power law behavior in the persistence PDFs with the self-similar Richardson cascading mechanism, given the implied scale-invariance associated with power-law distributions.^{51,78} Accordingly, it also explains the reduction in the extension of the power-law behavior for the w' signal associated with the near-neutral stability. From Table I, it is clear that the near-neutral stability class ($0 < -\zeta < 0.2$) corresponds only to the lowest three levels of the SLTEST experiment ($z = 1.4$ m, 2.1 m, 3 m). The inertial subrange of the w spectra starts approximately at $\kappa z = 1$, considering $\Lambda_w \approx z$. If this is converted to frequency ($f = \bar{u}/2\pi z$), then we would obtain the threshold at ≈ 1 Hz (assuming $\bar{u} \approx 10$ m s⁻¹ and $z = 2$ m), indicating only a decade wide subrange being resolved at the 20-Hz sampling rate. Therefore, the decrease in the power-law range for the w' signal could be attributed to insufficient sampling of small-scale eddies at 20-Hz frequency for the lowest three SLTEST levels.

3. Physical explanation of persistence exponents

In general, the exponents of the power-laws in persistence PDFs are non-trivial and difficult to compute analytically, except for simple systems such as fractional Brownian motions.^{1,4,5} Recently, to explain these power-law exponents, Cava and Katul²³ and Cava *et al.*²⁴ proposed an ambitious connection with the self-organized criticality (SOC) observed in the sandpile model of Bak, Tang, and Wiesenfeld.^{79,80} This is inspired by the results from Sreenivasan, Bershanskii, and Niemela⁸¹ where such a connection was proposed for turbulent convection. By using the results from Jensen, Christensen, and Fogedby⁸² and Bershanskii *et al.*,¹⁸ Cava *et al.*²⁴ connected these power-law exponents as

$$m = 3 - \gamma - \frac{\mu}{2}, \quad (14)$$

where m is the spectral slope of the telegraphic approximated time series, γ is the power-law exponent, and μ is the intermittency exponent. In a near-neutral atmospheric surface layer flow, Sreenivasan and Bershanskii¹⁹ found m to be equal to $4/3$, as opposed to the $5/3$ spectral slope in the inertial subrange.

If we accept this premise of SOC and assume m to be the same for u' , w' , and T' signals, then we can rewrite Eq. (14) as

$$\gamma = 1.67 - \frac{\mu}{2}, \quad (15)$$

where m is replaced as $4/3$. From Eq. (15), one can infer that the difference in the power-law exponents (γ) for u' , w' , and T' signals is directly related to the different values of the intermittency exponents (μ). Since we note that, from Figs. 2 and 7, the power-law exponent is the largest for the u' signal ($\gamma = 1.6$), Eq. (15) implies that the value of μ corresponding to this signal is the smallest, equal to 0.14. On the other hand, the power-law exponents for T' and w' signals are equal to $\gamma = 1.4$ and 1.25, respectively. Therefore, according to Eq. (15), the intermittency exponents for these two signals are considerably

larger than the u' signal, with the values being equal to 0.54 and 0.84 respectively.

Bershadskii *et al.*¹⁸ interpreted that the larger the intermittency exponent, there is more intermittent build-up of energy at the small scales, causing deviation from the Kolmogorov scaling for the higher-order structure functions (anomalous scaling) in the inertial subrange. Katul, Parlange, and Chu⁸³ and Katul *et al.*⁸⁴ demonstrated that in a convective surface layer, the temperature fluctuations are more intermittent compared to the velocity fluctuations, given the presence of sharp drops associated with the cliffs of the ramp-cliff patterns. Even though Eq. (15) dictates that the μ values for T' signals are larger than u' signals, there is also an implication that the μ values are the largest for w' signals, given their γ being the smallest ($\gamma = 1.25$). The reason for this difference is not clear at present.

Nevertheless, it is important to note that the one-to-one correspondence between the persistence and intermittency exponents as shown in Eq. (15) is predicated upon the assumption that the m values are equal for all three signals. Cava *et al.*²⁴ found that there is a considerable scatter among the m values for u' , w' , and T' signals in a convective surface layer and they often differ from $4/3$. Regardless, further discussion of the difference in persistence exponents among u' , w' , and T' signals is beyond the scope of this article.

However, an alternate theoretical framework also exists where the persistence PDFs are connected to the fractal dimensions of small-scale turbulence.^{85–87} In retrospect, this alternate framework had been proposed to provide a new methodology to compute the fractal dimensions, without relying on the box-counting methods being used in the studies by Sreenivasan and Meneveau⁸⁸ and Scotti, Meneveau, and Saddoughi⁸⁹ (see the work of Sreenivasan⁹⁰ and Catrakis⁹¹ for a review). Nonetheless, at present, both of these frameworks based on SOC and fractals seem plausible to connect these power-law exponents with the physical nature of small-scale turbulence, but further research is required to assess their viability. We present our conclusions in Sec. IV.

IV. CONCLUSION

We report the statistical scaling properties of the persistence PDFs of turbulent fluctuations in streamwise and vertical velocity (u' and w') and temperature (T') from the SLTEST experimental dataset in a convective surface layer. The important results from this study can be summarized as follows:

1. The persistence PDFs of u' , w' , and T' signals display a power-law behavior up to a certain threshold scale, punctuated with an exponential cutoff. The power-law exponents are 1.6, 1.25, and 1.4 for u' , w' , and T' signals, respectively, with no significant change being observed with stability.
2. From randomization experiments, it is shown that this power-law behavior of the persistence PDFs is linked to the temporal coherence in the time series. This temporal coherence is represented by the integral scales, computed from the autocorrelation functions.
3. By normalizing the persistence time scales with the integral scales, it is found that the power-law behavior in the PDFs is related to those scales that are smaller than the integral scales. Since power-laws are synonymous with scale-invariance, it

implies the effect of the self-similar eddy cascading mechanism (Richardson cascade) on the persistence PDFs.

4. A premultiplied form of the persistence PDF is used to demonstrate that the non-Gaussian effects of the temperature fluctuations act only at those scales that are larger than the integral scales. This indicates that the non-Gaussian characteristics of the temperature fluctuations are associated with the energy containing scales of motions.
5. From the exponential fits in the persistence CDFs, it is illustrated that the mean time scales of the negative T' events persisting longer than the integral scales are approximately twice the size of the integral scales in highly convective conditions. However, this mean time scale gradually decreases to almost being equal to the integral scale in the near-neutral stability.
6. On the other hand, for the long positive T' events, the mean time scales remain roughly equal to the integral scales, irrespective of stability. This discrepancy with the negative T' events is interpreted to be associated with the change in the topology of the coherent structures from cellular convection patterns in highly convective conditions to horizontal streaks in near-neutral stability.

Note that this study is the first of its kind for a convective surface layer turbulence, where the entire focus has been on establishing the statistical characteristics of the persistence PDFs. We have convincingly demonstrated that the persistence PDFs of velocity and temperature fluctuations in a convective surface layer follow a power-law distribution followed by an exponential cutoff. Subsequently, by scaling the persistence time scales with the integral scales, this statistical property of the persistence PDFs has been associated with the turbulent structures in a convective flow. Apparently, this scaling has been formulated by generating surrogate datasets that preserve or destroy the temporal correlations in a turbulent signal.

Apart from that, it is also important to emphasize that the findings obtained from this study have direct bearings on the quadrant behavior of the turbulent momentum and heat fluxes. This is because the switching patterns from one quadrant to the other are related to the combination of the zero-crossings in the component signals that construct the fluxes (u' and w' or w' and T'). Since the persistence PDFs are related to the time spent between the zero-crossings in a signal, the future research questions are as follows:

1. How the persistence PDFs of the heat and momentum fluxes are related to the persistence PDFs of the velocity and temperature fluctuations?
2. How much of the flux variation can be described by the persistence properties of the component signals?

AUTHORS' CONTRIBUTIONS

All the authors contributed equally to this work.

SUPPLEMENTARY MATERIAL

See the [supplementary material](#) for additional figures.

ACKNOWLEDGMENTS

The Indian Institute of Tropical Meteorology (IITM) is an autonomous institute fully funded by the Ministry of Earth Sciences, Government of India. S. Chowdhuri gratefully acknowledges the Director, IITM, Dr. Thara Prabhakaran, Dr. Shivsai Ajit Dixit, and Mr. Siddharth Kumar for the constant encouragement and stimulating discussions during the research. T. Banerjee acknowledges the funding support from the University of California Laboratory Fees Research Program funded by the UC Office of the President (UCOP) (Grant No. LFR-20-653572). Additional support was provided by the new faculty start up grant provided by the Department of Civil and Environmental Engineering, the Henry Samueli School of Engineering, University of California, Irvine. Dr. Kalmár-Nagy acknowledges funding from the Higher Education Excellence Program of the Ministry of Human Capacities in the frame of the Water Science & Disaster Prevention research area of Budapest University of Technology and Economics (Grant No. BME FIKP-VÍZ) and from the National Research, Development, and Innovation Fund (Grant No. TUDFO/51757/2019-ITM, Thematic Excellence Program). The authors are also immensely grateful to Dr. Keith G. McNaughton for kindly providing them the SLTEST dataset for this research. The authors also express their gratitude to the anonymous reviewers and the editor whose comments helped to improve the quality of this article. The computer codes used in this study are available to all the researchers by contacting the authors.

APPENDIX A: THE EFFECT OF BINNING ON PERSISTENCE PDFS

The common method for computing the PDFs of a stochastic variable is to bin the data in the linear space and computing the fraction of samples lying within each bin, divided by the bin-width.^{92,93} However, in the context of a stochastic variable that varies over a substantial range, sometimes many orders of magnitude, the linear binning may not be a good strategy. The PDFs obtained from linear binning for such variables are usually dominated by a few high probability bins at the lower range and an overwhelming amount of many low probability bins at the higher range, as illustrated by Dorval.⁵⁶ A better strategy is to use logarithmic binning for stochastic variables that have positively skewed distributions, such as having high densities at the lower range and low densities at the large range of values.⁵⁶ Intuitively, we may expect the same with the persistence time, having large occurrences associated with smaller time scales, with occasional incidences persisting for a long time.

In the logarithmic binning exercise, a logarithmic transformation is applied to the associated variable and then the fractions of samples are computed in each logarithmic bin, divided by the bin-width in the logarithmic space to compute the PDFs. The logarithmic binning has been used extensively to deduce the characteristics of the distributions associated with neuronal inter-spike intervals in biophysical signals,^{56,94} to estimate the size distribution of the avalanches associated with sandpile models,⁵⁰ and to identify the Lévy flight patterns in animal displacements^{53,54} and in many other practical cases (see Ref. 51 and the references therein for a detailed review on this topic).

However, the logarithmic bin-width is variable in the linear space and increases as the values increase, thus making the number of samples in each logarithmic bin dependent on the linear

width of the bin.⁵⁵ By employing the change of variables technique, Dorval⁵⁶ showed that the PDFs constructed in the linear (P_{lin}) and logarithmic (P_{log}) spaces are related to each other as

$$P_{\text{log}}(x) = (\log_e 10)[xP_{\text{lin}}(x)], \quad (\text{A1})$$

where x is the associated stochastic variable and the factor $\log_e 10$ emerges as the bins of x are constructed in powers of 10. Note that in this study, we also used the bins in power of 10 while constructing the persistence PDFs. Since the PDFs should be related to constant bin-width in the linear space,^{53,92} we can rearrange Eq. (A1) to obtain the actual PDFs from the logarithmic PDFs as

$$P(x) = [P_{\text{log}}(x)](x \log_e 10)^{-1}. \quad (\text{A2})$$

An alternate way to obtain the actual PDFs is to divide the fraction of samples within each logarithmic bin by the equivalent linear width in the logarithmic space, also known as normalized logarithmic binning.⁵⁵ However, both of these methods yield the same result, since the PDFs obtained from the normalized logarithmic binning are equivalent to Eq. (A2).

In Fig. 8, we show an example of persistence PDFs for u' , w' , and T' signals (combining both the positive and negative fluctuations) from a highly convective stability class ($-\zeta > 2$) to illustrate the effect of linear and logarithmic binning strategies. Before constructing the PDFs, the persistence time t_p is normalized by the integral scale Γ associated with u' , w' , and T' signals due to the reasons as described in Sec. III. We note that the linear PDFs and the PDFs described by Eq. (A2) are equivalent to each other, although the PDFs obtained from Eq. (A2) display a broader range of power-law behavior and are substantially less noisy than the linear PDFs in the larger range of t_p/Γ values. On the other hand, the logarithmic PDFs are pre-multiplied PDFs as shown in Eq. (A1). Therefore, compared to the actual PDFs, the logarithmic PDFs exhibit a flatter slope in the smaller range of t_p/Γ values, concomitant with a slower decrease in the larger range.

APPENDIX B: DESCRIPTION OF PHASE-RANDOMIZATION AND RANDOMIZATION EXPERIMENTS

To perform the phase-randomization experiment at varying strength of randomization, we first choose a 30-min time series of u' , w' , or T' signals (having 36 000 points at the sampling frequency of 20-Hz) from a particular stability class, as outlined in Table I. The step-by-step methodology is provided as follows:

1. The Fourier transformation of the 30-min time series is performed, generating 36 000 complex Fourier coefficients. Out of the 36 000 coefficients, half of these are the complex conjugates of each other, implying the need to only consider the Fourier phases of the first 18 000 coefficients.
2. These 18 000 Fourier phases are separated into two parts along their midpoint at the 9000th point. From the left half of the 9000 Fourier phases, $(\frac{x}{2})\%$ of the phases are randomly chosen, with the same being repeated for the right half as well.
3. These $(\frac{x}{2})\%$ of the randomly chosen phases from the left and right halves are shuffled with each other. Therefore, the total $x\%$ Fourier phases of the 18 000 coefficients are scrambled in this procedure while keeping their amplitudes intact. The revised Fourier coefficients are computed by using the same

amplitude but the scrambled phases, and then, their complex conjugates are taken for the rest of the 18 000 points.

- The inverse Fourier transform is undertaken for these revised Fourier coefficients to generate the phase-randomized time series at an $x\%$ randomization strength. The randomization strength implies the percentage of the Fourier phases that have been shuffled randomly to generate the surrogate dataset.

Note that the aforementioned procedure can be adopted for the randomization experiment as well. To generate a randomized dataset at an $x\%$ randomization strength, $(\frac{x}{2})\%$ of the time series values are randomly shuffled between the left and right halves, along the midpoint of the time series at 18 000th point. This type of shuffling procedure is known as Hurst's card simulation by drawing analogy with the shuffling patterns of a standard deck employed in card playing games.⁹⁵

DATA AVAILABILITY

The data that support the findings of this study are available from the corresponding author upon reasonable request.

REFERENCES

- S. N. Majumdar, "Persistence in nonequilibrium systems," *Curr. Sci.* **77**, 370–375 (1999).
- A. J. Bray, S. N. Majumdar, and G. Schehr, "Persistence and first-passage properties in nonequilibrium systems," *Adv. Phys.* **62**, 225–361 (2013).
- G. M. Molchan, "Maximum of a fractional Brownian motion: Probabilities of small values," *Commun. Math. Phys.* **205**, 97–111 (1999).
- F. Aurzada and C. Baumgarten, "Persistence of fractional Brownian motion with moving boundaries and applications," *J. Phys. A: Math. Theor.* **46**, 125007 (2013).
- F. Aurzada and T. Simon, "Persistence probabilities and exponents," in *Lévy Matters V* (Springer, 2015), pp. 183–224.
- G. Wang, G. Antar, and P. Devynck, "The Hurst exponent and long-time correlation," *Phys. Plasmas* **7**, 1181–1183 (2000).
- P. Perlekar, S. S. Ray, D. Mitra, and R. Pandit, "Persistence problem in two-dimensional fluid turbulence," *Phys. Rev. Lett.* **106**, 054501 (2011).
- D. Sornette, *Critical Phenomena in Natural Sciences: Chaos, Fractals, Self-Organization and Disorder: Concepts and Tools* (Springer Science and Business Media, 2006).
- B. Zheng, "Persistence probability in financial dynamics," *Mod. Phys. Lett. B* **16**, 775–782 (2002).
- A. Corral, "Long-term clustering, scaling, and universality in the temporal occurrence of earthquakes," *Phys. Rev. Lett.* **92**, 108501 (2004).
- D. S. Grebenkov, D. Holcman, and R. Metzler, "Preface: New trends in first-passage methods and applications in the life sciences and engineering," *J. Phys. A: Math. Theor.* **53**, 190301 (2020).
- S. O. Rice, "Mathematical analysis of random noise," *Bell Syst. Tech. J.* **24**, 46–156 (1945).
- K. R. Sreenivasan, A. Prabhu, and R. Narasimha, "Zero-crossings in turbulent signals," *J. Fluid Mech.* **137**, 251–272 (1983).
- R. A. Antonia, H. Q. Danh, and A. Prabhu, "Bursts in turbulent shear flows," *Phys. Fluids* **19**, 1680–1686 (1976).
- M. A. B. Narayanan, S. Rajagopalan, and R. Narasimha, "Experiments on the fine structure of turbulence," *J. Fluid Mech.* **80**, 237–257 (1977).
- D. Poggi and G. G. Katul, "Evaluation of the turbulent kinetic energy dissipation rate inside canopies by zero- and level-crossing density methods," *Boundary-Layer Meteorol.* **136**, 219–233 (2010).
- P. Kailasnath and K. R. Sreenivasan, "Zero crossings of velocity fluctuations in turbulent boundary layers," *Phys. Fluids* **5**, 2879–2885 (1993).
- A. Bershadskii, J. Niemela, A. Praskovskiy, and K. Sreenivasan, "Clusterization and intermittency of temperature fluctuations in turbulent convection," *Phys. Rev. E* **69**, 056314 (2004).
- K. R. Sreenivasan and A. Bershadskii, "Clustering properties in turbulent signals," *J. Stat. Phys.* **125**, 1141–1153 (2006).
- T. Kalmár-Nagy and Á. Varga, "Complexity analysis of turbulent flow around a street canyon," *Chaos, Solitons Fractals* **119**, 102–117 (2019).
- E. Yee, P. R. Kosteniuk, G. M. Chandler, C. A. Biltoft, and J. F. Bowers, "Statistical characteristics of concentration fluctuations in dispersing plumes in the atmospheric surface layer," *Boundary-Layer Meteorol.* **65**, 69–109 (1993).
- E. Yee, R. Chan, P. R. Kosteniuk, G. M. Chandler, C. A. Biltoft, and J. F. Bowers, "Measurements of level-crossing statistics of concentration fluctuations in plumes dispersing in the atmospheric surface layer," *Boundary-Layer Meteorol.* **73**, 53–90 (1995).
- D. Cava and G. G. Katul, "The effects of thermal stratification on clustering properties of canopy turbulence," *Boundary-Layer Meteorol.* **130**, 307 (2009).
- D. Cava, G. Katul, A. Molini, and C. Elefante, "The role of surface characteristics on intermittency and zero-crossing properties of atmospheric turbulence," *J. Geophys. Res. Atmos.* **117**, D01104, <https://doi.org/10.1029/2011jd016167> (2012).
- G. I. Barenblatt, *Scaling, Self-Similarity, and Intermediate Asymptotics: Dimensional Analysis and Intermediate Asymptotics* (Cambridge University Press, 1996), Vol. 14.
- P. A. Davidson, *Turbulence: An Introduction for Scientists and Engineers* (Oxford University Press, 2015).
- G. G. Katul, J. Albertson, M. Parlange, C.-R. Chu, and H. Stricker, "Conditional sampling, bursting, and the intermittent structure of sensible heat flux," *J. Geophys. Res. Atmos.* **99**, 22869–22876, <https://doi.org/10.1029/94jd01679> (1994).
- C. M. A. Pinto, A. M. Lopes, and J. A. Tenreiro Machado, "Double power laws, fractals and self-similarity," *Appl. Math. Model.* **38**, 4019–4026 (2014).
- R. Narasimha, S. R. Kumar, A. Prabhu, and S. V. Kailas, "Turbulent flux events in a nearly neutral atmospheric boundary layer," *Philos. Trans. R. Soc., A* **365**, 841–858 (2007).
- M. Chamecki, "Persistence of velocity fluctuations in non-Gaussian turbulence within and above plant canopies," *Phys. Fluids* **25**, 115110 (2013).
- M. Metzger, B. J. McKeon, and H. Holmes, "The near-neutral atmospheric surface layer: Turbulence and non-stationarity," *Philos. Trans. R. Soc. Lond.* **365**, 859–876 (2007).
- H. Panosfsky and J. Dutton, *Atmospheric Turbulence: Models and Methods for Engineering Applications* (John Wiley & Sons, 1984).
- J. C. Kaimal and J. J. Finnigan, *Atmospheric Boundary Layer Flows: Their Structure and Measurement* (Oxford University Press, 1994).
- T. Foken and C. J. Napo, *Micrometeorology* (Springer, 2008), Vol. 2.
- S. Chowdhuri, K. G. McNaughton, and T. V. Prabha, "An empirical scaling analysis of heat and momentum cospectra above the surface friction layer in a convective boundary layer," *Boundary-Layer Meteorol.* **170**, 257–284 (2019).
- S. Chowdhuri, S. Kumar, and T. Banerjee, "Revisiting the role of intermittent heat transport towards Reynolds stress anisotropy in convective turbulence," *J. Fluid Mech.* (in press) (2020).
- A. Donato, D. Cava, and D. Contini, "A case study of the performance of different detrending methods in turbulent-flux estimation," *Boundary-Layer Meteorol.* **164**, 19–37 (2017).
- J. C. Kaimal, J. C. Wyngaard, Y. Izumi, and O. R. Coté, "Spectral characteristics of surface-layer turbulence," *Q. J. R. Meteorol. Soc.* **98**, 563–589 (1972).
- B. A. Kader, A. M. Yaglom, and S. L. Zubkovskii, "Spatial correlation functions of surface-layer atmospheric turbulence in neutral stratification," *Boundary-Layer Meteorol.* **47**, 233–249 (1989).
- B. Kader and A. Yaglom, "Spectra and correlation functions of surface layer atmospheric turbulence in unstable thermal stratification," in *Turbulence and Coherent Structures* (Springer, 1991), pp. 387–412.
- K. G. McNaughton and J. Laubach, "Power spectra and cospectra for wind and scalars in a disturbed surface layer at the base of an advective inversion," *Boundary-Layer Meteorol.* **96**, 143–185 (2000).
- T. Banerjee and G. G. Katul, "Logarithmic scaling in the longitudinal velocity variance explained by a spectral budget," *Phys. Fluids* **25**, 125106 (2013).

- ⁴³K. Ghannam, G. G. Katul, E. Bou-Zeid, T. Gerken, and M. Chamecki, "Scaling and similarity of the anisotropic coherent eddies in near-surface atmospheric turbulence," *J. Atmos. Sci.* **75**, 943–964 (2018).
- ⁴⁴A. Monin and A. Yaglom, *Statistical Fluid Mechanics: Mechanics of Turbulence* (MIT Press, 1971), Vol. 1.
- ⁴⁵H. Tennekes and J. Lumley, *A First Course in Turbulence* (MIT Press, 1972).
- ⁴⁶Y. Malhi, K. McNaughton, and C. Von Randow, "Low frequency atmospheric transport and surface flux measurements," in *Handbook of Micrometeorology* (Springer, 2004), pp. 101–118.
- ⁴⁷K. G. McNaughton, "Attached eddies and production spectra in the atmospheric logarithmic layer," *Boundary-Layer Meteorol.* **111**, 1–18 (2004).
- ⁴⁸K. G. McNaughton, "Turbulence structure of the unstable atmospheric surface layer and transition to the outer layer," *Boundary-Layer Meteorol.* **112**, 199–221 (2004).
- ⁴⁹G. E. Willis and J. W. Deardorff, "On the use of Taylor's translation hypothesis for diffusion in the mixed layer," *Q. J. R. Meteorol. Soc.* **102**, 817–822 (1976).
- ⁵⁰K. Christensen and N. R. Moloney, *Complexity and Criticality* (World Scientific Publishing Company, 2005), Vol. 1.
- ⁵¹M. E. J. Newman, "Power laws, Pareto distributions and Zipf's law," *Contemp. Phys.* **46**, 323–351 (2005).
- ⁵²S. Pueyo, "Diversity: Between neutrality and structure," *Oikos* **112**, 392–405 (2006).
- ⁵³D. W. Sims, D. Righton, and J. W. Pitchford, "Minimizing errors in identifying Lévy flight behaviour of organisms," *J. Anim. Ecol.* **76**, 222–229 (2007).
- ⁵⁴S. Benhamou, "How many animals really do the lévy walk?," *Ecology* **88**, 1962–1969 (2007).
- ⁵⁵E. P. White, B. J. Enquist, and J. L. Green, "On estimating the exponent of power-law frequency distributions," *Ecology* **89**, 905–912 (2008).
- ⁵⁶A. Dorval, "Estimating neuronal information: Logarithmic binning of neuronal inter-spike intervals," *Entropy* **13**, 485–501 (2011).
- ⁵⁷M. G. Newberry and V. M. Savage, "Self-similar processes follow a power law in discrete logarithmic space," *Phys. Rev. Lett.* **122**, 158303 (2019).
- ⁵⁸H. Nakagawa and I. Nezu, "Prediction of the contributions to the Reynolds stress from bursting events in open-channel flows," *J. Fluid Mech.* **80**, 99–128 (1977).
- ⁵⁹G. Katul, C.-I. Hsieh, G. Kuhn, D. Ellsworth, and D. Nie, "Turbulent eddy motion at the forest-atmosphere interface," *J. Geophys. Res. Atmos.* **102**, 13409–13421, <https://doi.org/10.1029/97jd00777> (1997).
- ⁶⁰C. R. Chu, M. B. Parlange, G. G. Katul, and J. D. Albertson, "Probability density functions of turbulent velocity and temperature in the atmospheric surface layer," *Water Resour. Res.* **32**, 1681–1688, <https://doi.org/10.1029/96wr00287> (1996).
- ⁶¹L. Liu, F. Hu, and X. Cheng, "Probability density functions of turbulent velocity and temperature fluctuations in the unstable atmospheric surface layer," *J. Geophys. Res. Atmos.* **116**, D12117, <https://doi.org/10.1029/2010jd015503> (2011).
- ⁶²A. Garai and J. Kleissl, "Interaction between coherent structures and surface temperature and its effect on ground heat flux in an unstably stratified boundary layer," *J. Turbul.* **14**, 1–23 (2013).
- ⁶³R. Lyu, F. Hu, L. Liu, J. Xu, and X. Cheng, "High-order statistics of temperature fluctuations in an unstable atmospheric surface layer over grassland," *Adv. Atmos. Sci.* **35**, 1265–1276 (2018).
- ⁶⁴R. J. Adrian, R. T. D. S. Ferreira, and T. Boberg, "Turbulent thermal convection in wide horizontal fluid layers," *Exp. Fluids* **4**, 121–141 (1986).
- ⁶⁵S. Chowdhuri, T. V. Prabha, A. Karipot, T. Dharamraj, and M. N. Patil, "Relationship between the momentum and scalar fluxes close to the ground during the indian post-monsoon period," *Boundary-Layer Meteorol.* **154**, 333–348 (2015).
- ⁶⁶S. Chowdhuri and T. V. Prabha, "An evaluation of the dissimilarity in heat and momentum transport through quadrant analysis for an unstable atmospheric surface layer flow," *Environ. Fluid Mech.* **19**, 513–542 (2019).
- ⁶⁷M. Santhanam and H. Kantz, "Return interval distribution of extreme events and long-term memory," *Phys. Rev. E* **78**, 051113 (2008).
- ⁶⁸D. Poggi and G. Katul, "Flume experiments on intermittency and zero-crossing properties of canopy turbulence," *Phys. Fluids* **21**, 065103 (2009).
- ⁶⁹G. Lancaster, D. Iatsenko, A. Pidde, V. Ticcinelli, and A. Stefanovska, "Surrogate data for hypothesis testing of physical systems," *Phys. Rep.* **748**, 1–60 (2018).
- ⁷⁰T. Maiwald, E. Mammen, S. Nandi, and J. Timmer, "Surrogate data—A qualitative and quantitative analysis," in *Mathematical Methods in Signal Processing and Digital Image Analysis* (Springer, 2008), pp. 41–74.
- ⁷¹J. Wyngaard, *Turbulence in the Atmosphere* (Cambridge University Press, 2010).
- ⁷²G. Katul, C.-I. Hsieh, and J. Sigmon, "Energy-inertial scale interactions for velocity and temperature in the unstable atmospheric surface layer," *Boundary-Layer Meteorol.* **82**, 49–80 (1997).
- ⁷³D. Li, G. G. Katul, and E. Bou-Zeid, "Mean velocity and temperature profiles in a sheared diabatic turbulent boundary layer," *Phys. Fluids* **24**, 105105 (2012).
- ⁷⁴K. G. McNaughton, R. Clement, and J. Moncrieff, "Scaling properties of velocity and temperature spectra above the surface friction layer in a convective atmospheric boundary layer," *Nonlinear Process. Geophys.* **14**, 257 (2007).
- ⁷⁵T. Banerjee, G. G. Katul, S. T. Salesky, and M. Chamecki, "Revisiting the formulations for the longitudinal velocity variance in the unstable atmospheric surface layer," *Q. J. R. Meteorol. Soc.* **141**, 1699–1711 (2015).
- ⁷⁶S. Khanna and J. G. Brasseur, "Three-dimensional buoyancy- and shear-induced local structure of the atmospheric boundary layer," *J. Atmos. Sci.* **55**, 710–743 (1998).
- ⁷⁷S. T. Salesky, M. Chamecki, and E. Bou-Zeid, "On the nature of the transition between roll and cellular organization in the convective boundary layer," *Boundary-Layer Meteorol.* **163**, 41–68 (2017).
- ⁷⁸M. K. Verma, S. Manna, J. Banerjee, and S. Ghosh, "Universal scaling laws for large events in driven nonequilibrium systems," *Europhys. Lett.* **76**, 1050 (2006).
- ⁷⁹P. Bak, C. Tang, and K. Wiesenfeld, "Self-organized criticality: An explanation of the 1/f noise," *Phys. Rev. Lett.* **59**, 381–384 (1987).
- ⁸⁰P. Bak, C. Tang, and K. Wiesenfeld, "Self-organized criticality," *Phys. Rev. A* **38**, 364 (1988).
- ⁸¹K. R. Sreenivasan, A. Bershadskii, and J. J. Niemela, "Multiscale soc in turbulent convection," *Physica A* **340**, 574–579 (2004).
- ⁸²H. J. Jensen, K. Christensen, and H. C. Fogedby, "1/f noise, distribution of lifetimes, and a pile of sand," *Phys. Rev. B* **40**, 7425 (1989).
- ⁸³G. G. Katul, M. B. Parlange, and C. R. Chu, "Intermittency, local isotropy, and non-Gaussian statistics in atmospheric surface layer turbulence," *Phys. Fluids* **6**, 2480–2492 (1994).
- ⁸⁴G. G. Katul, M. B. Parlange, J. D. Albertson, and C. R. Chu, "Local isotropy and anisotropy in the sheared and heated atmospheric surface layer," *Boundary-Layer Meteorol.* **72**, 123–148 (1995).
- ⁸⁵H. J. Catrakis and P. E. Dimotakis, "Scale distributions and fractal dimensions in turbulence," *Phys. Rev. Lett.* **77**, 3795 (1996).
- ⁸⁶P. E. Dimotakis and H. J. Catrakis, "Turbulence, fractals, and mixing," in *Mixing* (Springer, 1999), pp. 59–143.
- ⁸⁷H. J. Catrakis, "Distribution of scales in turbulence," *Phys. Rev. E* **62**, 564 (2000).
- ⁸⁸K. R. Sreenivasan and C. Meneveau, "The fractal facets of turbulence," *J. Fluid Mech.* **173**, 357–386 (1986).
- ⁸⁹A. Scotti, C. Meneveau, and S. G. Saddoughi, "Fractal dimension of velocity signals in high-Reynolds-number hydrodynamic turbulence," *Phys. Rev. E* **51**, 5594 (1995).
- ⁹⁰K. R. Sreenivasan, "Fractals and multifractals in fluid turbulence," *Annu. Rev. Fluid Mech.* **23**, 539–604 (1991).
- ⁹¹H. J. Catrakis, "The multiscale-minima meshless (M3) method: A novel approach to level crossings and generalized fractals with applications to turbulent interfaces," *J. Turbul.* **9**, N22 (2008).
- ⁹²H. Panofsky and G. Brier, *Some Applications of Statistics to Meteorology* (Pennsylvania State University, University Park, 1958).
- ⁹³J. Lumley, *Stochastic Tools in Turbulence* (Academic Press, 1970).
- ⁹⁴J. V. Selinger, N. V. Kulagina, T. J. O'Shaughnessy, W. Ma, and J. J. Pancrazio, "Methods for characterizing interspike intervals and identifying bursts in neuronal activity," *J. Neurosci. Methods* **162**, 64–71 (2007).
- ⁹⁵J. Strecker, Fractional Brownian motion simulation: Observing fractal statistics in the wild and raising them in captivity, 2004, <http://www.cs.umd.edu/strecker/jstreckerIS-pdflatex.pdf>.